

# A multi-channel model for an $\alpha$ plus ${}^6\text{He}$ nucleus cluster

K. Amos<sup>(1,4)\*</sup>, L. Canton<sup>(2)</sup>, P. R. Fraser<sup>(3)</sup>,  
S. Karataglidis<sup>(1,4)</sup>, J. P. Svenne<sup>(5)</sup>, and D. van der Knijff<sup>(1)</sup>

<sup>(1)</sup> *School of Physics, University of Melbourne, Victoria 3010, Australia*

<sup>(2)</sup> *Istituto Nazionale di Fisica Nucleare,  
Sezione di Padova, Padova I-35131, Italia*

<sup>(3)</sup> *Department of Physics, Astronomy and Medical Radiation Sciences,  
Curtin University, GPO Box U1987, Perth 6845, Australia*

<sup>(4)</sup> *Department of Physics, University of Johannesburg,  
P.O. Box 524 Auckland Park, 2006, South Africa and*

<sup>(5)</sup> *Department of Physics and Astronomy, University of Manitoba,  
and Winnipeg Institute for Theoretical Physics,  
Winnipeg, Manitoba, Canada R3T 2N2*

(Dated: July 6, 2021)

## Abstract

A multi-channel algebraic scattering (MCAS) method has been used to solve coupled sets of Lippmann-Schwinger equations for the  $\alpha+{}^6\text{He}$  cluster system, so finding a model spectrum for  ${}^{10}\text{Be}$  to more than 10 MeV excitation. Three states of  ${}^6\text{He}$  are included and the resonance character of the two excited states taken into account in finding solutions. A model Hamiltonian has been found that gives very good agreement with the known bound states and with some low-lying resonances of  ${}^{10}\text{Be}$ . More resonance states are predicted than have as yet been observed. The method also yields  $S$ -matrices which we have used to evaluate low-energy  ${}^6\text{He}$ - $\alpha$  scattering cross sections. Reasonable reproduction of low-energy differential cross sections and of energy variation of cross sections measured at fixed scattering angles is found.

PACS numbers: 21.60Ev, 21.60Gx, 24.10Eq, 24.30Gd, 25.70Gh

---

\*Electronic address: amos@unimelb.edu.au

## I. INTRODUCTION

Nuclear reactions can and have been used as tests of models of nuclear structure, through analyses of data therefrom. In the low-energy regime, they are the primary energy-generation mechanisms in stars. However, in a stellar environ, those reactions typically take place at energies much lower than those accessible by laboratory experiments. For example, at stellar energies ( $\leq \sim 300$  keV), radiative capture rates are usually too small to be measured directly. Thus, estimates of reaction cross sections important in astrophysics application have to be extrapolated from data measured at higher energies. Theoretical extrapolations are difficult due to the size of uncertainties that accompany the lowest-energy results measured, as well as from any specific influence of resonances in the Gamow window regime. Nonetheless, some cases are suited to direct theoretical analysis by using few-body techniques. Three- and four-body systems can be treated by finding solutions of the Faddeev [1] and Faddeev-Yakubovsky [2] equations, respectively, with the later in the Alt-Grassberger-Sandhas form [3] and using realistic nucleon-nucleon interactions. However, calculations of scattering with these methods are technically complex.

There have been many attempts to theoretically establish microscopic models of both nuclear structure and reactions (see [4–6] for many references). In [5], one such theory was developed to specify the nuclear optical potential from first principles. An objective was to have a well established potential for use in evaluation of capture rates, especially of neutron capture rates on rare isotopes of nuclei; rates that are needed in simulations of cataclysmic events such as supernovae explosions. But, it has been noted [5] that only selected nuclei, and specific reaction channels, can be addressed with the various *ab-initio* methods so far developed.

Thus, it remains a standard approach to use phenomenological optical potentials between nuclear clusters, from which relative motion functions can be used to give capture cross sections at energies in the Gamow window. In most studies, local forms of phenomenological optical potentials have been used for simplicity. With stable nuclei, there exist global parameterisations obtained from fits to much data. However, the application of global parameterization parameter values to exotic nuclear systems is unreliable. Furthermore, optical potentials are known to be non-local due to the character of the underlying in-medium nucleon-nucleon interactions, the Pauli principle that results in exchange scattering amplitudes, and specific coupled-channel effects. These features have been described [7], and at low energies, the role of coupled-channels has been shown [8] to be more complex than the approximate treatment of nonlocality via the Perey effect [9].

However, if coupled-channel and Pauli principle effects can be taken into account, local phenomenological nuclear interactions remain useful for any simplicity they give in evaluations. As an example, a phenomenological two-cluster model with a local two-nucleus interaction [4] has been used to describe low energy scattering and properties of the compound system bound states. The Pauli principle was taken into account in the multi-nucleon systems by considering group representations of the ground states of individual elements of the cluster as well as of the compound. Using a sum of Gaussians for the two-nuclei interactions, fairly good descriptions of low energy nucleon-nucleus and  $\alpha$ -nucleus scattering data were found. Of note, the potential parameters were partial wave dependent so that for the  $\alpha$  and light nuclei systems,  $s$ ,  $p$ ,  $d$ - and  $f$ -partial waves contribute to the cross sections, even for energies of few MeV.

In this paper, we report on studies made in a similar vein, using a multi-channel algebraic

scattering method (MCAS) to calculate low energy scattering of two nuclei and the low excitation spectrum of their compound (bound and resonant). Local forms are taken for the interactions for the coupled-channel problem and allowance for the effects of the Pauli principle has been made. In particular we report results of an application of the MCAS method to consider  $^{10}\text{Be}$  as a coupled-channel problem of an  $\alpha$ - $^6\text{He}$  cluster. We consider the coupling to be with three low-excitation states (the ground and two resonance states) of  $^6\text{He}$ . Besides giving a spectrum for  $^{10}\text{Be}$ , the MCAS programs also have been used to predict low-energy cross sections for  $^6\text{He}$ - $\alpha$  elastic scattering. Results are compared to a number of the measured data sets [10] taken for a small range of energies and for various scattering angles.

The experimental results from the low-energy scattering of  $^6\text{He}$  ions off  $\alpha$  particles [10] are of great interest since the  $^6\text{He}$  nucleus is weakly bound and is deemed to have an extended neutron distribution that has been termed a ‘halo’. The  $\alpha$  particle, in contrast, is strongly bound with its first excited state at over 20 MeV excitation. The compound system,  $^{10}\text{Be}$ , is also quite strongly bound with the  $\alpha$ + $^6\text{He}$  threshold lying at 7.413 MeV in the spectrum. Given that the  $\alpha$ + $\alpha$  compound,  $^8\text{Be}$ , is unbound, the two additional neutrons weakly bound in  $^6\text{He}$  are attached in covalent bounding orbits in the cluster of that nucleus with an  $\alpha$  to form  $^{10}\text{Be}$ .

The nucleus  $^6\text{He}$  lies close to the neutron drip line. Its ground state lies 0.973 MeV below the two neutron break-up threshold and that state  $\beta^-$  decays. The next two states are resonances with energy centroids of 1.797 and 5.6 MeV [11] and they decay by two neutron (equivalently  $\alpha$ ) emissions. The first excited resonance state is narrow (113 keV) while the second is quite broad (12 MeV [11]). Such properties have had impact in cluster model evaluations of spectra of other compound systems [12–15].

In the following section, we specify the model we have used to define the matrix of potentials for the coupled-channel problem. Then in Sec. III we report the spectra found with it for  $^{10}\text{Be}$  treated as an  $\alpha$ + $^6\text{He}$  cluster. In Sec. IV, we present and discuss elastic scattering cross sections of  $^6\text{He}$  ions scattering from an  $\alpha$ -particle at low c.m. energies. Conclusions are given in Sec. V.

## II. THE MODEL FOR THE $\alpha$ -NUCLEUS MATRIX OF POTENTIALS

The  $\alpha$ - $^6\text{He}$  matrix of potentials have been defined using a rotational collective model for the interaction [16]. The potential assumed in describing the cluster system is allowed to have central ( $V_0$ ),  $\ell^2$ -dependent ( $V_{\ell\ell}$ ), and orbit-nuclear spin ( $V_{\ell I}$ ) components. This potential is also taken to have quadrupole deformation.

There is an additional interaction considered to account for pair correlations that affect the energies of  $0^+$  states  $^{10}\text{Be}$ . BCS theory, developed for the description of superconductivity, was found very useful in treating the effect of pairing interactions in even-mass nuclei, and delineating the consequences of correlations induced by those interactions. In symbolic form, Hamiltonians have been taken as

$$H = H_0 + H_{pair} + H_{Q.Q},$$

where  $H_0$  is the part of the Hamiltonian that describes single-particle motion in a self-consistent potential supplemented by pairing ( $H_{pair}$ ) and quadrupole-quadrupole ( $H_{Q.Q}$ ) forces. In Chapter 11 of Ref. [17] on pairing force theory, it is shown that a pairing interaction of monopole type leads to additional binding in nuclear (ground) states of even

mass nuclei, and is considered to cause the even-odd  $A$  mass difference. Concomitantly, it can yield a large energy gap between the ground  $0^+$  and first excited states (usually a  $2^+$ ). Additionally, from studies of collectivity in heavy nuclei [18, 19], the mutual interplay between dynamical pairing and quadrupole correlations explained anomalously low excitation energies of excited  $0^+$  states. With light nuclei, and  $^{10}\text{Be}$  in particular, a two-phonon pairing vibrational ( $2p - 2h$ ) state is anticipated to lie at an energy of 4.8 MeV above the ground state [20]; an energy which emerges directly from two differences in binding energies, namely  $[(\text{BE}(^{10}\text{Be}) - \text{BE}(^8\text{Be})) - (\text{BE}(^{12}\text{Be}) - \text{BE}(^{10}\text{Be}))]$ . Pairing and correlation effects then are relevant, particularly in defining the location of the  $0^+$  states in the spectrum of  $^{10}\text{Be}$  when treated as an  $\alpha + ^6\text{He}$  cluster. With the quite simple collective model form we use, those additional properties are approximated by using a monopole potential acting in all channels leading to  $0^+$  states in the compound system.

To outline the MCAS method, consider a basis of channel states defined by the coupling

$$|c\rangle = |\ell I J^\pi\rangle = \left[ |\ell\rangle \otimes |\psi_I\rangle \right]_J^{M,\pi}, \quad (1)$$

where  $\ell$  is the orbital angular momentum of relative motion of a spin-0 projectile on the target whose states are  $|\psi_I^{(N)}\rangle$ . With each  $J^\pi$  hereafter understood, and by disregarding deformation temporarily, the ( $\alpha$ -nucleus) potential matrices may be written

$$V_{cc'}(r) = \langle \ell I | W(r) | \ell' I' \rangle = \left[ V_0 \delta_{c'c} f(r) + V_{\ell\ell} f(r) [\ell \cdot \ell] + V_{II} f(r) [\mathbf{I} \cdot \mathbf{I}] + V_{\ell I} g(r) [\ell \cdot \mathbf{I}] \right]_{cc'} + V_{\text{mono}} \delta_{c'c} \delta_{J^\pi=0^+} f(r), \quad (2)$$

in which local form factors have been assumed. Typically they are specified as Woods-Saxon functions,

$$f(r) = \left[ 1 + e^{\left(\frac{r-R}{a}\right)} \right]^{-1} \quad ; \quad g(r) = \frac{1}{r} \frac{df(r)}{dr}. \quad (3)$$

Deformation then is included with the nuclear surface defined by

$$R = R(\theta, \phi) = R_0(1 + \epsilon), \quad (4)$$

where, for a rotational model of the target and in the space-fixed frame,

$$\epsilon = \sum_L \sqrt{\frac{4\pi}{(2L+1)}} \beta_L [\mathbf{Y}_L(\Omega) \cdot \mathbf{Y}_L(\zeta)]; \quad (5)$$

$\beta_L$  are deformation parameters and  $\zeta$  are the Euler angles for the transformation from the body-fixed to space-fixed frames.  $\Omega = (\theta, \phi)$  are the angles defining the surface in the space-fixed frame. Expanding  $f(r - R(\theta, \phi)) = f(r - R_0(1 + \epsilon))$  to order  $\epsilon^2$  gives

$$f(r) \rightarrow f_0(r) + \epsilon \left[ \frac{df(r)}{d\epsilon} \right]_0 + \frac{1}{2} \epsilon^2 \left[ \frac{d^2 f(r)}{d\epsilon^2} \right]_0 = f_0(r) - R_0 \frac{df_0(r)}{dr} \epsilon + \frac{1}{2} R_0^2 \frac{d^2 f_0(r)}{dr^2} \epsilon^2, \quad (6)$$

There is a similar equation for  $g(r)$ .

When collective models are used to specify the matrix of interaction potentials acting between a nuclear projectile and a set of states of a target nucleus, there are problems in

satisfying the Pauli principle [21]. In the MCAS method the effects of the Pauli principle are met by inclusion of a set of orthogonalizing pseudo-potentials (OPP) [22]; a technique that was developed in studies of cluster physics [23, 24] as a variant of the Orthogonality Condition Model of Saito [25]. It accounted for the effects of Pauli blocking in the relative motion of two clusters comprised of fermion constituents. The OPP can also be used for the situation with partially occupied levels being Pauli hindered. Schmid [26] notes that states can be Pauli-forbidden, Pauli-allowed, or Pauli-suppressed; the last being what we have called Pauli hindrance in previous applications of MCAS [27, 28].

To orthogonalize states describing intra-cluster motion with respect to the deeply-bound Pauli forbidden states, MCAS uses highly nonlocal OPP terms embedded in a coupled-channel context. The matrix of interaction potentials (in coordinate space) to be used has the form

$$\mathcal{V}_{cc'} = V_{cc'}(r)\delta(r - r') + \lambda_c A_c(r)A_{c'}(r')\delta_{cc'}. \quad (7)$$

$V_{cc'}(r)$  is the nuclear interaction potential and  $\lambda_c$  is the scale, in MeV, used to satisfy the Pauli principle. Pauli blocking of the specific orbit in a particular channel,  $c$ , is achieved by using a very large  $\lambda_c$  value. That value should be infinite but for all practical purposes  $10^6$  MeV suffices. Pauli allowed states have  $\lambda_c = 0$ . Pauli hindrance has values  $0 < \lambda_c < \infty$  ( $10^6$ ). The  $A_c(r)$  are bound state wave functions (of the  $\alpha$  in this application) associated with the diagonal nuclear interactions  $V_{cc}(r)$  for the relevant orbital angular momentum in each channel  $c$ .

### III. $^{10}\text{Be}$ AS A COUPLED $\alpha+^6\text{He}$ SYSTEM

This system is of interest given the (relatively) recent experimental studies of the elastic scattering of  $^6\text{He}$  from an  $\alpha$  target [10], as well as of resonant  $\alpha$  capture on  $^6\text{He}$ , which seek limits on clustering in states of the compound,  $^{10}\text{Be}$ . We have used the coupled-channel Hamiltonian described above to find as good a representation of the spectrum of  $^{10}\text{Be}$  as possible, up to the first break-up threshold (of  $n+^9\text{Be}$ ) at 6.812 MeV and just beyond. The  $\alpha+^6\text{He}$  threshold lies at 7.413 MeV above the ground state. To 6.812 MeV excitation there are six known states, of which four have positive, and two negative, parity. Two more states (one of each parity) lie at excitations close to these thresholds and the rest have energy centroids greater than 9.2 MeV in the spectrum. Thus, all low-excitation resonances in  $^{10}\text{Be}$ , save for the  $3_1^-$  one at 7.31 MeV, may decay by particle emission of a neutron and/or an  $\alpha$ -particle.

In the MCAS evaluations, the coupled-channel Hamiltonians were formed assuming that there were three states of relevance in the spectrum of  $^6\text{He}$ . They are the ground ( $0^+$ ) that  $\beta^-$  decays and the two excited resonance states that decay by two neutron break-up. The first resonance has a  $2^+$  spin-parity while the second is uncertain [11]. We choose it to have a  $2^+$  spin-parity as was the case when using MCAS to find a good spectrum for  $^7\text{Li}$  treated as a  $p+^6\text{He}$  cluster [29]. The  $2_1^+$  and  $2_2^+$  states, being particle-unstable resonances, have the assigned shape of a Lorentzian multiplied by a projectile-energy dependant scaling factor, which has the form of a Wigner distribution. This eliminates erroneous threshold and sub-threshold behaviour inherent in a pure Lorentzian form. As necessary with such widths, an energy-dependant correction is added to the target-state centroids to restore causality. Full details are available in Ref. [15]. The  $^6\text{He}$  states' properties, along with the strengths of the OPP by which the  $\alpha$  particle orbits are hindered, are shown in Table I.

TABLE I: The states of  ${}^6\text{He}$  used in the coupled-channel evaluations. With all states the  $\alpha$   $s$ -orbit was presumed blocked using  $\lambda_{1s} = 10^6$  in the OPP. All energies are in units of MeV.

state	Centroid	Width	OPP ( $\lambda_{1p}$ )	OPP ( $\lambda_{1d}$ )	OPP ( $\lambda_{2s}$ )
$0_{\text{g.s.}}^+$	0.000	0.00	10.915	0.0	3.3
$2_1^+$	1.797	0.113	11.1	4.7	0.75
$2_2^+$	5.60	12.0	9.42	0.0	0.0

The coupled-channel matrix of potentials defining the Hamiltonian was specified by a collective rotational model with the parameter set listed in Table II. Shown at the bottom

TABLE II: The potential parameters used for the interactions in the  $\alpha+{}^6\text{He}$  system. All strengths are in MeV and lengths are in fermi.

Pot. strengths	Negative	Positive	Geometry
$V_0$	-42.13	-41.85	$R_0 = 2.58$
$V_{\ell\ell}$	1.14	1.14	$a_0 = 0.7$
$V_{\ell I}$	1.07	1.07	$\beta_2 = 0.7$
$V_{II}$	1.4	0.4	
$V_{\text{mono}}$		-7.72	
Coulomb (charge dist.)			
${}^6\text{He}$	$R_c = 1.3$	${}^4\text{He}$	$R_c = 1.008$
	$a_c = 0.4$		$a_c = 0.327$
	$w_c = 0.31$		$w_c = 0.445$

of Table II are the parameter values of a three parameter Fermi (3pF) model we have used to define the charge distributions of  ${}^4,6\text{He}$  in generating the Coulomb potentials in the Hamiltonian. The 3pF charge distribution is of the form

$$\rho_{ch}(r) = \rho_0 \frac{1 + w_c \left(\frac{r}{R_c}\right)^2}{1 + \exp\left(\frac{r-R_c}{a_c}\right)}. \quad (8)$$

For an  $\alpha$  particle, the parameters were determined by a fit to the electron scattering form factor at low momentum [30]. No such data exist as yet for  ${}^6\text{He}$ , though analysis of the isotope shift of spectral lines [31] gives a root-mean-square (rms) charge radius of 2.054 fm, and we select a 3pF parameter set consistent with that value. Details of our use of these charge distributions are given in Appendix A.

Using MCAS for the  $\alpha+{}^6\text{He}$  cluster gave the spectrum for  ${}^{10}\text{Be}$  identified with the label ‘MCAS’ in Fig. 1. For clarity, we separate the positive and negative parity states in the spectra on the left and right side of this figure. The results are compared with the known spectrum, labelled ‘exp.’. Of note is that, save for the uncertain assigned spin-parity of ( $4^-$ ), every known state has a matching partner in the calculated spectrum with excitation energies in quite good agreement. For comparison, we have found a spectrum for  ${}^{10}\text{Be}$  from shell model calculations made using the WBT interaction [32] with the OXBASH

program [33]. A no-core calculation was made by using a single particle basis consisting of all single nucleon states from the  $0s$ -shell up to, and including, the  $(0h1f2p)$ -shell. In this way, the full six major shells have been taken into account. Positive parity states have been determined using the complete  $(0 + 2 + 4)\hbar\omega$  space while those for negative parity states were made in a  $(1 + 3)\hbar\omega$  space. The results are shown in the columns labelled ‘SM’. In the

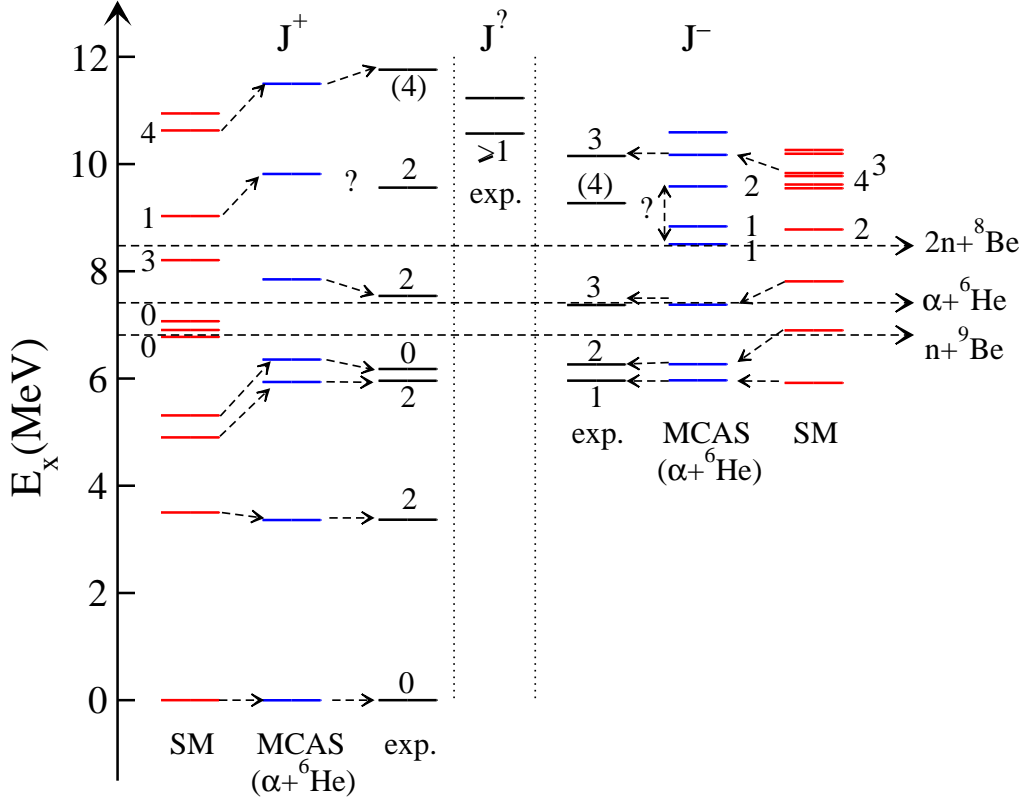


FIG. 1: (Color online) The low excitation spectra for  $^{10}\text{Be}$  found from the shell model calculations (left), from the data tabulation [34] (center), and from the MCAS evaluations (left). Positive (negative) parity states are grouped on the left (right) of this figure.

shell model spectrum, there are additional positive parity states,  $(0_3^+, 3^+, 1^+)$  states within 1.5 MeV above the  $\alpha$  emission threshold, while there are additional negative parity states  $(2_2^-, 0^-, 1_2^-, 1_3^-)$  in the region to  $\sim 10$  MeV excitation.

Hence, both model results find reasonable to good agreement with the known low-excitation spectrum; finding the eight known states to within  $\sim 1$  MeV of their listed energy values. Both evaluations, however, give a number of (unobserved) levels, especially in the immediate region above the break-up thresholds. Those thresholds indicated on the diagram are for neutron ( $n+^9\text{Be}$ ; 6.812 MeV),  $\alpha$  ( $\alpha+^6\text{He}$ ; 7.413 MeV) and two-neutron ( $2n+^8\text{Be}$ ; 8.478 MeV) emissions.

Known properties of the low-excitation states in  $^{10}\text{Be}$  (energies and widths) are also compared with the results of the MCAS evaluation in Table III. Here it must be noted that, as the known resonances except for the  $3_1^-$  state lie above the  $n+^9\text{Be}$  threshold, the calculated widths are partial ones, and those for the decay  $^{10}\text{Be} \rightarrow n+^9\text{Be}$  need be added to make a proper comparison with the known values.

With MCAS, the match between the calculated and experimental spectra  $^{10}\text{Be}$  is very

TABLE III: The known and MCAS evaluated spectrum of  $^{10}\text{Be}$ . All energies are in units of MeV relative to the  $\alpha+^6\text{He}$  threshold.

$J^\pi$	$E_{Exp.}$	$\Gamma_{Exp.}$	$J^\pi$	$E_{MCAS}$	$\Gamma_{MCAS}$
$0^+$	<b>-7.413</b>			<b>-7.421</b>	
$2^+$	<b>-4.048</b>			<b>-4.059</b>	
$2^+$	<b>-1.458</b>			<b>-1.485</b>	
$1^-$	<b>-1.456</b>			<b>-1.452</b>	
$0^+$	<b>-1.237</b>			<b>-1.065</b>	
$2^-$	<b>-1.153</b>			<b>-1.153</b>	
$3^-$	<b>-0.045</b>			<b>-0.042</b>	
$2^+$	<b>0.126</b>	0.006		<b>0.429</b>	0.006
			$1^-$	1.085	0.539
$(4^-)$	1.854	0.154	$1^-$	1.417	0.059
$2^+$	2.144	0.141	$2^-$	2.164	0.130
			$1^+$	2.395	0.277
$3^-$	<b>2.734</b>	0.296		<b>2.710</b>	0.119
$\geq 1$	<b>3.157</b>	?	$1^-$	<b>3.172</b>	0.998
?	3.817	0.200			
$4^+$	<b>4.347</b>	0.121		<b>4.077</b>	$5 \times 10^{-4}$

The question marks indicate that no value is given in the table [34].

good up to  $\sim 8$  MeV. The calculated energies of all (known) states in the region agree to within a few tens of keV, and we emphasise those by bold type in the table. The  $3_2^-$  resonances has a matching MCAS results, with a centroid only 24 keV from the established value and a well-matching centroid. The observed  $2_4^+$  state does not have a partner, with the same parity, though a  $2^-$  state is calculated with an energy difference of 20 keV and an almost identical width.

To achieve these results with MCAS required

- A ‘pairing correlation effect’ (monopole) components in the  $\alpha$ - $^6\text{He}$  interaction. This was needed to provide extra binding for the  $0_{1,2}^+$  states of the compound system  $^{10}\text{Be}$ . A shift of  $\sim 2$  MeV from the values found with no monopole term, was required.
- An OPP hindrance term for the  $1p$ -orbit of the  $\alpha$  in each of the three target states. They only influence the results for the negative parity states in  $^{10}\text{Be}$ , but were needed both to find the correct sequence of spin-parities and the energy separations of the three bound states.
- An OPP hindrance term for the  $1d$ -orbit of the  $\alpha$  in the  $^6\text{He}$   $2_1^+$  state. This was necessary to increase the energy of the  $^{10}\text{Be}$   $4^+$  resonance to near experiment. Without it, this state had an energy of  $\sim 7$  MeV.
- The chosen width of the  $2_2^+$  resonance state in  $^6\text{He}$ , influences the positive parity spectrum of  $^{10}\text{Be}$  in the resonance region. However only when the value is quite small is there noticeable variations in the spectrum.



- Varying the positive parity interaction strengths gave the following effects:
  1. Setting  $V_{II}^{(+)} = 0$  changed the energies of all but that of the  $2_1^+$  by less than 0.4 MeV, and that of the ground not at all. The  $2_1^+$  state, however became much more bound.
  2. Setting  $V_{\ell I}^{(+)} = 0$  hardly affected the energies of the ground ( $0^+$ ) and  $2_1^+$  states, but others varied by as much as  $\pm 1$  MeV.
  3. Setting  $V_{\ell\ell}^{(+)} = 0$  did not affect the binding energy of the ground state but changes those of all others noticeably, most becoming much more bound.
- while, for the negative parity spectrum,
  1. Setting  $V_{II}^{(-)} = 0$  changed all but the binding of the  $2_1^-$  state by less than  $-0.3$  MeV. The  $2_1^-$  state however was much more bound.
  2. Setting  $V_{\ell I}^{(-)} = 0$  gave only minor changes with states being more bound by less than 0.2 MeV.
  3. Setting  $V_{\ell\ell}^{(-)} = 0$  made most states more bound; an effect equivalent to increasing the depth of the central component.
  4. The Pauli hindrance of the relative motion  $p$ -orbit was crucial in finding the energies and splitting of the lowest two negative parity states in particular. Removing this hindrance lead to the  $1_1^-$  state dropping in energy to become the ground state.

#### IV. SCATTERING OF ${}^6\text{He}$ IONS FROM $\alpha$ PARTICLES

Data from elastic (and inelastic) scattering of a  ${}^6\text{He}$  radioactive ion beam from  $\alpha$ -particles have been reported recently [10] at low energies suitable for analysis using MCAS. Data, both in the form of angular distributions at fixed energies and differential energy cross sections for select angle values, have been taken for a range of center of mass (c.m.) energies from  $\sim 2$  to 6 MeV. With respect to the spectrum of the compound  ${}^{10}\text{Be}$ , this energy range (above threshold) coincides with an excitation energy  $\sim 9.4$  to 13.4 MeV.

With the coupled-channel Hamiltonian defined to best represent the known sub-threshold states in  ${}^{10}\text{Be}$ , numerous resonance states are found with higher energies. The resonance states with well-known  $J^\pi$  in  ${}^{10}\text{Be}$  lying above the  $\alpha+{}^6\text{He}$  threshold (7.41 MeV), and with centroid energies defined with respect to that threshold, are the  $2_3^+$  with centroid (width) of 0.126 (0.006) MeV, the  $2_4^+$  at 2.144 (0.141) MeV, and the  $3_2^-$  at 2.734 (0.141) MeV. There are also states with an uncertainly assigned  $4^-$  and  $4^+$   $J^\pi$ , one with  $J \geq 1$  and no assigned parity, and one with no assignment. All might influence  $\alpha$ - ${}^6\text{He}$  scattering cross sections in the low c.m. energy range. From Fig. 1, it is evident that MCAS gives a rather rich spectrum above the particle emission thresholds, dominantly of negative parity resonances; states that have not been observed. The MCAS results for the two known resonances give very good matches for the energy centroids. Regarding widths, the  $2_3^+$  result is extremely close to that observed, but the calculated width of the  $3_2^-$  resonance is less than half of that observed, and that for the  $4^+$  is much smaller than observed. The calculated width of the  $2_1^-$  resonance is very near that of the  $2_4^+$  resonance observed very near the same energy. Thus with this MCAS model, while we expect some effects in cross-section evaluations due

to these resonances, there is much to be uncertain about regarding how well the calculated spectrum matches the physical states at these energies. Much depends on how the resonances relate to the  $\alpha$  scattering from the ground state of  ${}^6\text{He}$ .

### A. Differential cross sections at fixed energies

In Fig. 2, angular distribution data [10] taken at six energies are compared with MCAS results. We have used data uncertainties as listed in the tabulations of the experimental results [35]. The energies at which each of the data sets have been taken and at which each of the MCAS evaluations were made are indicated in the figure. With the exception

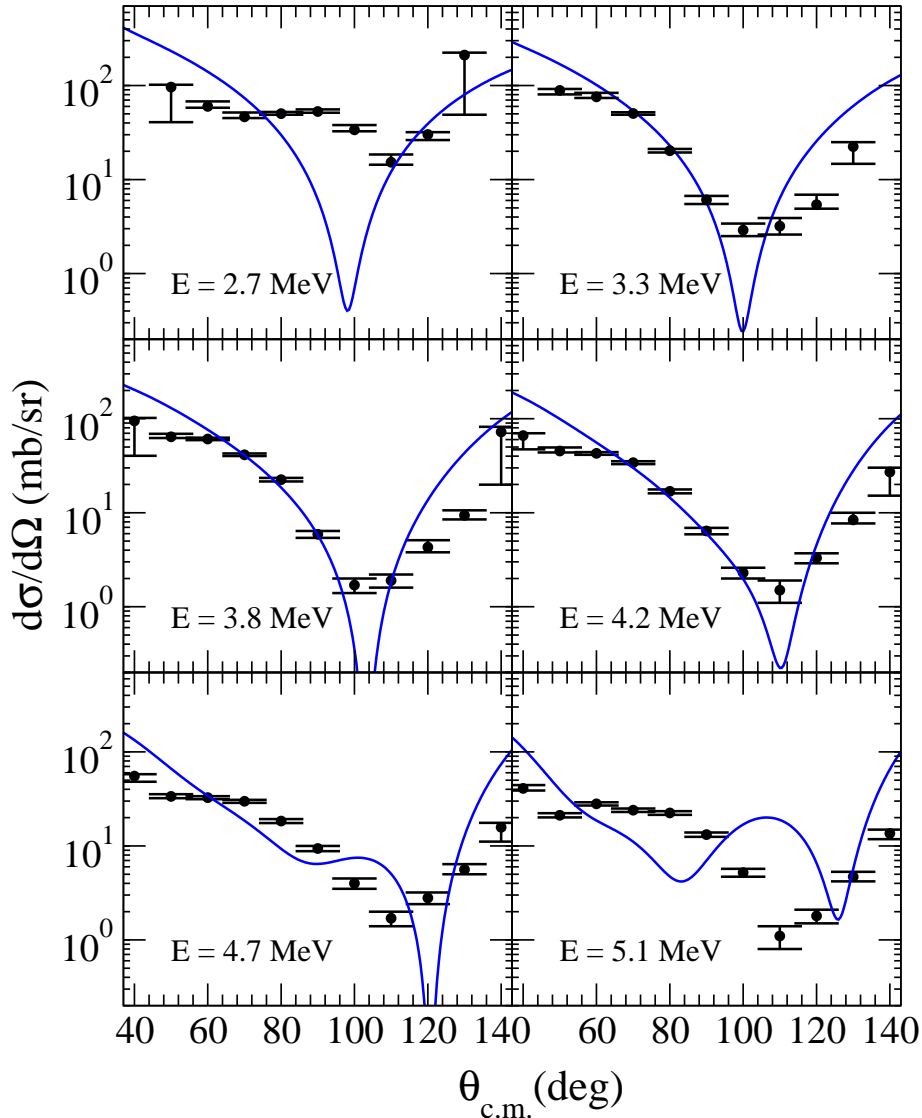


FIG. 2: (Color online) Angular distributions at various fixed energies as listed compared with data [10].

of the 2.7 MeV result, the calculated cross sections are in reasonable agreement with the data, having appropriate magnitudes and tracking the shape of the cross section data. The

2.7 MeV data are distinctly different to the other energy data sets (and of the MCAS expectation) and the known  $2_4^+$  resonance in  $^{10}\text{Be}$  (2.12 MeV) has a marked effect. MCAS finds state with the correct angular momentum and width at an energy close to that observed, but with incorrect parity. As that resonance may not have the same shape as a function of energy as that observed, the calculated 2.7 MeV cross section result is then not surprisingly a poor representation of measured data. Further, in the 5.1 MeV result, and arguably the 4.7 MeV result, there are calculated minima and maxima not observed in the data.

### B. Energy variations at fixed scattering angles

Data for energy variations of cross sections measured in two ranges of scattering angles,  $65\text{-}75^\circ$  and  $95\text{-}105^\circ$ , are shown in Fig. 3, compared to calculated MCAS results. In the top panel, it is shown that the  $65^\circ$  result overestimates the cross section until  $\sim 4.5$  MeV, after which it underestimates it. The  $75^\circ$  result is lower than all but the two lowest-energy data points. Both show a dip at  $\sim 5.5$  MeV not seen in the data, but are otherwise as featureless as the observed cross section. In the bottom panel, the curves depict the MCAS results found for scattering angles of  $95^\circ$  (solid) and  $105^\circ$  (dashed). These are results spanning the region of the minima of the differential cross sections; this is revealed by the marked difference in their shapes. Save for the resonance-like effect in data in the 2-3 MeV range, the  $95^\circ$  result is a reasonable representation of the data, considering that this concerns minima in the cross-sections (as observed in the fixed energy data). The  $105^\circ$  result contains more minima and maxima than observed, and at most energies is a poor match to data.

### C. Partial wave terms in the coupled-channels evaluations

In Fig. 4, the cross section taken at 3.8 MeV is compared with individual components from the MCAS evaluation. As indicated, the pure Coulomb cross section for the scattering of the two  $3pF$  charge distributions is shown by the solid curve. When the calculated  $s$ -wave scattering amplitudes are added to that, the cross section shown by the long-dashed curve results. Adding the  $p$ -wave scattering amplitudes gives the cross section depicted by the small-dashed curve; and which features a minima near  $100^\circ$ . This is observed also in full calculated result with  $d$ - and  $f$ -waves included (solid curve), though it is deeper. Clearly the  $p$ -wave scattering arising from the couple channel calculations define the increase in cross section values at backward scattering angles.

## V. CONCLUSIONS

The MCAS method has been used to solve coupled sets of Lippmann-Schwinger equations for the  $\alpha+^6\text{He}$  cluster, finding a model spectrum for  $^{10}\text{Be}$  in good agreement with the known one to more than 10 MeV excitation. A collective model was used to define the input matrix of interaction potentials for the coupled-channel problem in which three positive-parity states in  $^6\text{He}$  were involved. Two of those states were taken to be resonances themselves, with widths as defined in a data tabulation [11]. The effect of the Pauli principle on the relative motion of the  $\alpha$  and  $^6\text{He}$  was taken into account using the OPP method. Pairing was accounted by using a monopole interaction between the  $\alpha$  and  $^6\text{He}$ . That was found to be

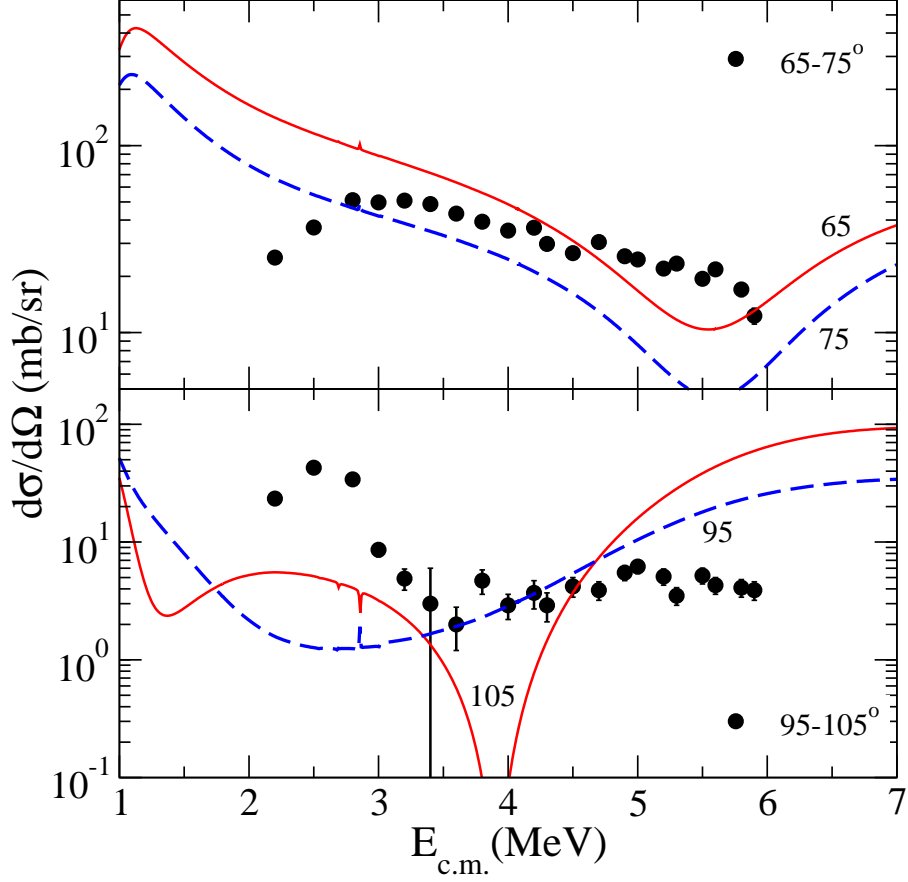


FIG. 3: (Color online) Energy variation of cross sections at the indicated scattering angles compared with data accumulated over 10 degree intervals [10].

necessary to give the known splitting between the ground state of the compound system,  $^{10}\text{Be}$ , and its excited states, notably the  $2_1^+$  and  $0_2^+$ .

Applying MCAS to specify scattering amplitudes for positive centre of mass energies gave angular distributions in reasonable agreement with measured data at most energies for which the shape and magnitude reflect a non-resonant character. The energy variation results are more diverse. For most energies, data taken in the range  $65 - 75^\circ$  is enveloped by cross sections evaluated at the extremes of the range, and the calculated results are almost as featureless as the data. For angles near where the minimum is observed in fixed-energy data, the  $95 - 105^\circ$  region, the results are of lower quality.

Overall, MCAS had produced a good representation of the  $^{10}\text{Be}$  spectrum (treated as an  $\alpha + ^6\text{He}$  cluster), with calculated state energies found to within a few keV of those observed across an 8 MeV interval. Calculated cross sections are a credible to good recreation of the available data.

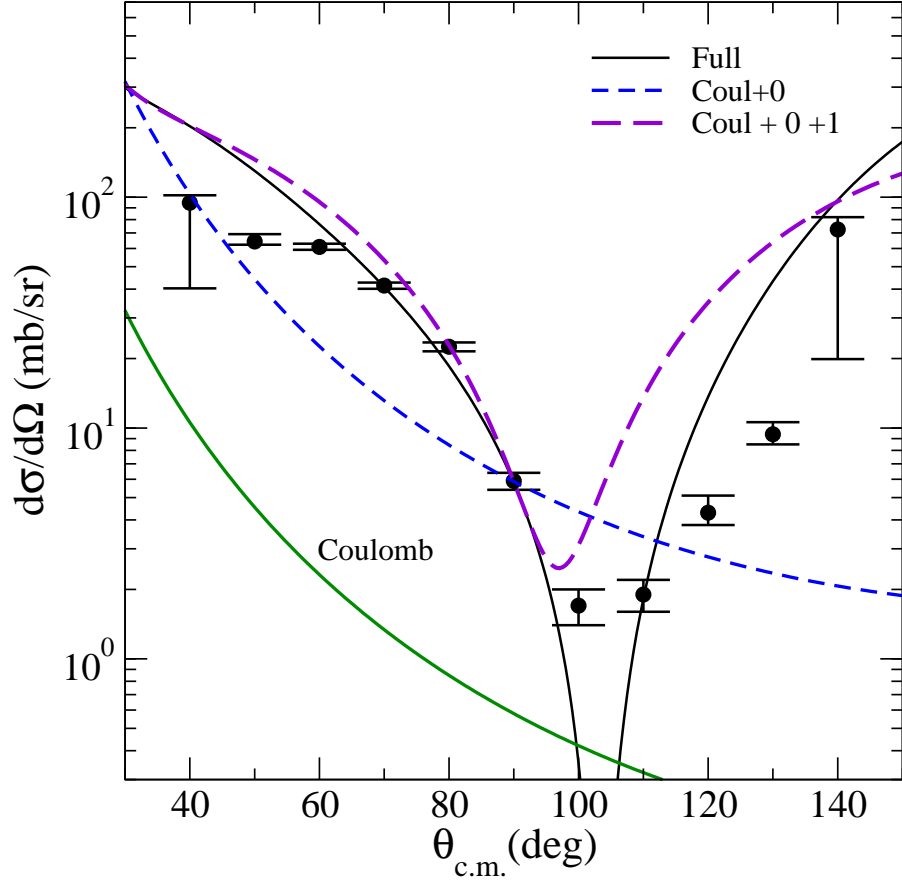


FIG. 4: (Color online) Partial wave contributions in the differential cross section measured at 3.8 MeV.

### Acknowledgments

SK acknowledges support from the National Research Foundation of South Africa.

- 
- [1] L. D. Faddeev, *Sov. Phys. JETP* **12**, 1014 (1961).
  - [2] O. A. Yakubovski, *Sov. J. Nucl. Phys.* **5**, 937 (1967).
  - [3] E. O. Alt, P. Grassberger, and W. Sandhas, *Nucl. Phys.* **B2**, 167 (1967).
  - [4] S. B. Dubovichenko and Y. N. Uzikov, *Physics of Particles and Nuclei* **42**, 251 (2011).
  - [5] J. Rotureauux, P. Danielewicz, G. Hagen, F. Nunes, and T. Papenbrock, arXiv: 1611:04554 [nucl-th] (2016).
  - [6] P. Navrátil, S. Quaglioni, G. Hupin, C. Romero-Redondo, and A. Calci, *Phys. Scr.* **91**, 053002 (2016).
  - [7] K. Amos, P. J. Dortmans, H. V. von Germab, S. Karataglidis, and J. Raynal, *Adv. in Nucl. Phys.* **25**, 275 (2000).
  - [8] P. R. Fraser, K. Amos, S. Karataglidis, L. Canton, G. Pisent, and J. P. Svenne, *Euro. Phys. J. A* **35**, 69 (2008).
  - [9] F. G. Perey and B. Buck, *Nucl. Phys.* **32**, 353 (1962).

- [10] D. Suzuki et al., Phys. Rev. C **87**, 054301 (2013).
- [11] D. R. Tilley et al., Nucl. Phys. **A 708**, 3 (2002).
- [12] P. Fraser, K. Amos, L. Canton, G. Pisent, S. Karataglidis, J. Svenne, and D. van der Knijff, Phys. Rev. Lett. **101**, 0242501 (2008).
- [13] L. Canton, P. R. Fraser, J. P. Svenne, K. Amos, S. Karataglidis, and D. van der Knijff, Phys. Rev. C **83**, 047603 (2011).
- [14] P. Fraser, L. Canton, R. Fossion, K. Amos, S. Karataglidis, J. Svenne, and D. van der Knijff, EPJ web of conferences **63**, 02010 (2013).
- [15] P. R. Fraser, K. Massen-Hane, K. Amos, I. Bray, L. Canton, R. Fossion, A. S. Kadyrov, S. Karataglidis, J. P. Svenne, and D. van der Knijff, Phys. Rev. C **94**, 034603 (2016).
- [16] T. Tamura, Rev. Mod. Phys. **37**, 679 (1965).
- [17] D. J. Rowe, *Nuclear Collective Motion* (World Scientific, Singapore, 2010).
- [18] S. Iwasaki, T. Marumori, F. Sakata, and K. Takada, Prog. Theor. Phys. **56**, 1140 (1976).
- [19] F. Sakata and G. Holzwarth, Prog. Theor. Phys. **61**, 1649 (1979).
- [20] F. Barranco, R. A. Broglia, G. Gori, E. Vigezzi, P. F. Bortignon, and J. Terasaki., Phys. Rev. Lett. **83**, 2147 (1999).
- [21] L. Canton, G. Pisent, J. P. Svenne, D. van der Knijff, K. Amos, and S. Karataglidis, Phys. Rev. Lett **94**, 122503 (2005).
- [22] K. Amos, L. Canton, G. Pisent, J. P. Svenne, and D. van der Knijff, Nucl. Phys. **A728**, 65 (2003), and references cited therein.
- [23] V. Krasnopol'sky and V. Kukulin, Soviet J. Nucl. Phys. **20**, 883 (1974).
- [24] V. Kukulin and V. Pomerantsev, Ann. of Phys. **111**, 330 (1978).
- [25] S. Saito, Prog. Theor. Phys. **41**, 705 (1969).
- [26] E. W. Schmidt, in *Proceedings of the workshop in few-body problems in nuclear physics* (Trieste, Italy, 1978), p. 389.
- [27] L. Canton, G. Pisent, J. P. Svenne, K. Amos, and S. Karataglidis, Phys. Rev. Lett **96**, 072502 (2006).
- [28] K. Amos, L. Canton, P. R. Fraser, S. Karataglidis, J. P. Svenne, and D. van der Knijff, Nucl. Phys. **A912**, 7 (2013).
- [29] L. Canton, G. Pisent, K. Amos, S. Karataglidis, J. P. Svenne, and D. van der Knijff, Phys. Rev. C **74**, 064605 (2006).
- [30] C. W. de Jager, H. de Vries, and C. de Vries, At. Data Nucl. Data Tables **14**, 479 (1974).
- [31] L.-B. Wang et al., Phys. Rev. Lett. **93**, 142501 (2004).
- [32] E. K. Warburton and B. A. Brown, Phys. Rev. C **46**, 923 (1992).
- [33] OXBASH-MSU (the Oxford-Buenos-Aries-Michigan State University shell model code). A. Etchegoyen, W.D.M. Rae, and N.S. Godwin (MSU version by B.A. Brown, 1986); B.A. Brown, A. Etchegoyen, and W.D.M. Rae, MSUCL Report Number 524 (1986).
- [34] D. R. Tilley et al., Nucl. Phys. **A 745**, 155 (2004).
- [35] [www.nndc.bnl.gov/exfor](http://www.nndc.bnl.gov/exfor).

## Appendix A: $\alpha$ - ${}^6\text{He}$ Coulomb potentials from two charge distributions

Three different forms for Coulomb potentials have been investigated, assuming that

1. both the  $\alpha$  and  ${}^6\text{He}$  are point charge particles (each with charge  $2e$ ),
2. that the  ${}^6\text{He}$  only had a three parameter Fermi (3pF) charge distribution, and

3. that both have 3pF charge distributions.

The 3pF charge distribution is of the form given in Eq. (8), namely

$$\rho_{ch}(r) = \rho_0 \frac{1 + w_c \left(\frac{r}{R_c}\right)^2}{1 + \exp\left(\frac{r-R_c}{a_c}\right)}. \quad (\text{A1})$$

For an  $\alpha$  particle, the parameters were determined by a fit to the electron scattering form factor at low momentum. Those values [30],  $R_c = 1.008$  fm,  $a_c = 0.327$  fm, and  $w_c = 0.445$ , gave a charge rms radius of  $R_{\text{rms}}^{(c)} = 1.7$  fm. The associated (unnormalised) charge distribution is shown by the solid curve in Fig. 5. The normalisation required is  $\rho_0 = 0.119$ .

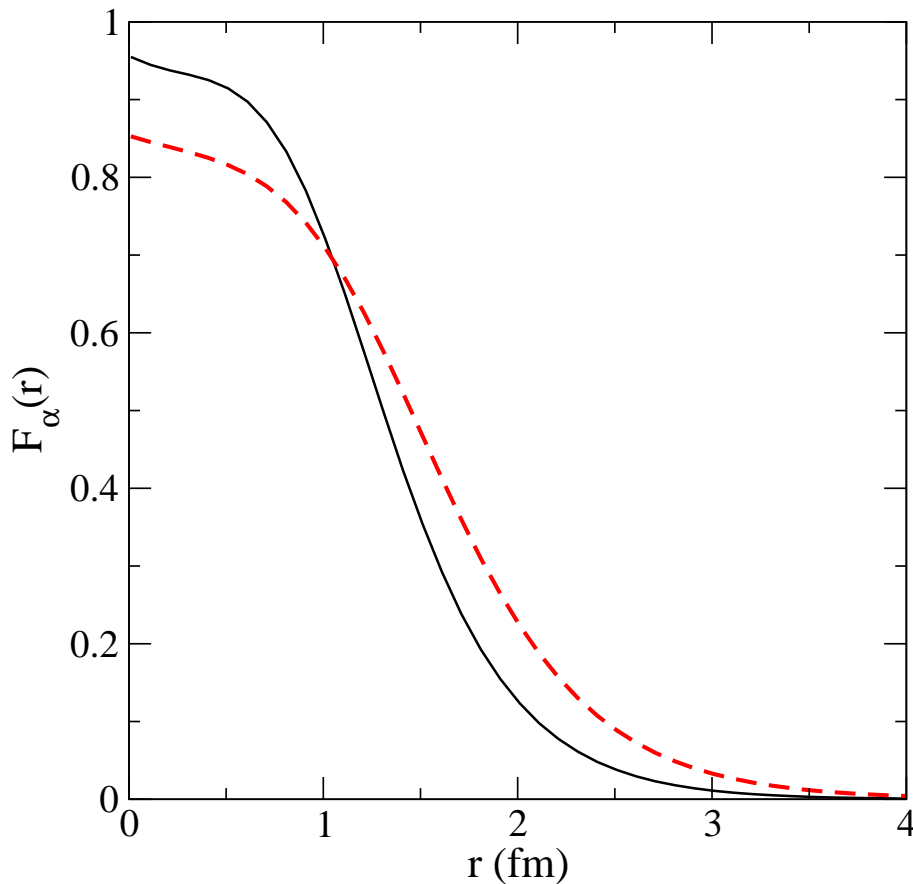


FIG. 5: (Color online) The three parameter charge distribution for an  $\alpha$  nucleus.

For  ${}^6\text{He}$ , it is now known [31] via a laser spectroscopic determination that its  $R_{\text{rms}}^{(c)} = 2.054$  fm. That result alone does not settle the actual charge distribution, but a range of values for a 3pF distribution that gives this value of  $R_{\text{rms}}^{(c)}$  is listed in Table IV. We choose the parameter set,  $R_c = 1.30$  fm,  $a_c = 0.40$  fm, and  $w_c = 0.31$  as the basic set for  ${}^6\text{He}$ , and for those, the charge distribution is shown by the dashed curve in Fig. 5. The central density required with this is  $\rho_0 = 0.0704$ .

With the (normalised) charge distributions, Coulomb potentials were obtained for each of the following three cases. They are

TABLE IV: Values of the parameters of 3pF charge distributions that have  $R_{\text{rms}}^{(c)} \sim 2.054$  fm.

ID	$R_c$	$a_c$	$w$	$a_c$	$w$
1	1.20	0.38	0.64	0.40	0.32
2	1.25	0.38	0.59	0.40	0.32
3	1.30	0.38	0.55	0.40	0.31
4	1.35	0.38	0.51	0.39	0.38
5	1.40	0.38	0.46	0.39	0.35
6	1.50	0.37	0.50	0.38	0.37
7	1.55	0.36	0.60	0.38	0.32
8	1.60	0.36	0.51	0.37	0.38
9	1.65	0.36	0.44	0.37	0.32

1. Case of two point charge particles:

The Coulomb potentials generated for this model is given simply by

$$V_{\text{coul}}(r) = \frac{4e^2}{r}. \quad (\text{A2})$$

It is shown in Fig. 6 by the dot-dashed curve.

2. Case where  ${}^6\text{He}$  alone is given by a 3pF charge distribution:

If a nucleus has a spherical charge distribution,  $\rho(\mathbf{r}') = \rho_0 f_{\text{coul}}(r')$ , then it is easily shown that the charge number  $Z$  is given by

$$Z = 4\pi\rho_0 \int_0^\infty f_{\text{coul}}(r') r'^2 dr', \quad (\text{A3})$$

thus defining the central charge density as

$$\rho_0 = Ze / \left[ 4\pi \int_0^\infty f_{\text{coul}}(r') r'^2 dr' \right]. \quad (\text{A4})$$

The Coulomb interaction felt by a positively charged point test particle (having charge  $2e$  for a point  $\alpha$ -particle) is

$$V_{\text{coul}}(r) = (2e) \int \rho_0 f(r') \frac{1}{|\mathbf{r}' - \mathbf{r}|} d\mathbf{r}' \quad (\text{A5})$$

and expanding in multipoles, the angular integration leaves only the  $s$ -wave ( $\ell = 0$ ) component whence

$$V_{\text{coul}}(r) = 2e(4\pi)\rho_0 \int_0^\infty F(r') v_{\ell=0}(r', r) r'^2 dr'. \quad (\text{A6})$$

where  $v_{\ell=0}(r', r) = 1/r_>$  where  $r_>$  being the greater of  $r'$  and  $r$ . Then the radial integration splits into two terms to give

$$V_{\text{coul}}(r) = 4\pi(2e)\rho_0 \left[ \frac{1}{r} \int_0^r f_{\text{coul}}(s) s^2 ds + \int_r^\infty \frac{1}{s} f_{\text{coul}}(s) s^2 ds \right] (= \mathcal{V}_\alpha). \quad (\text{A7})$$



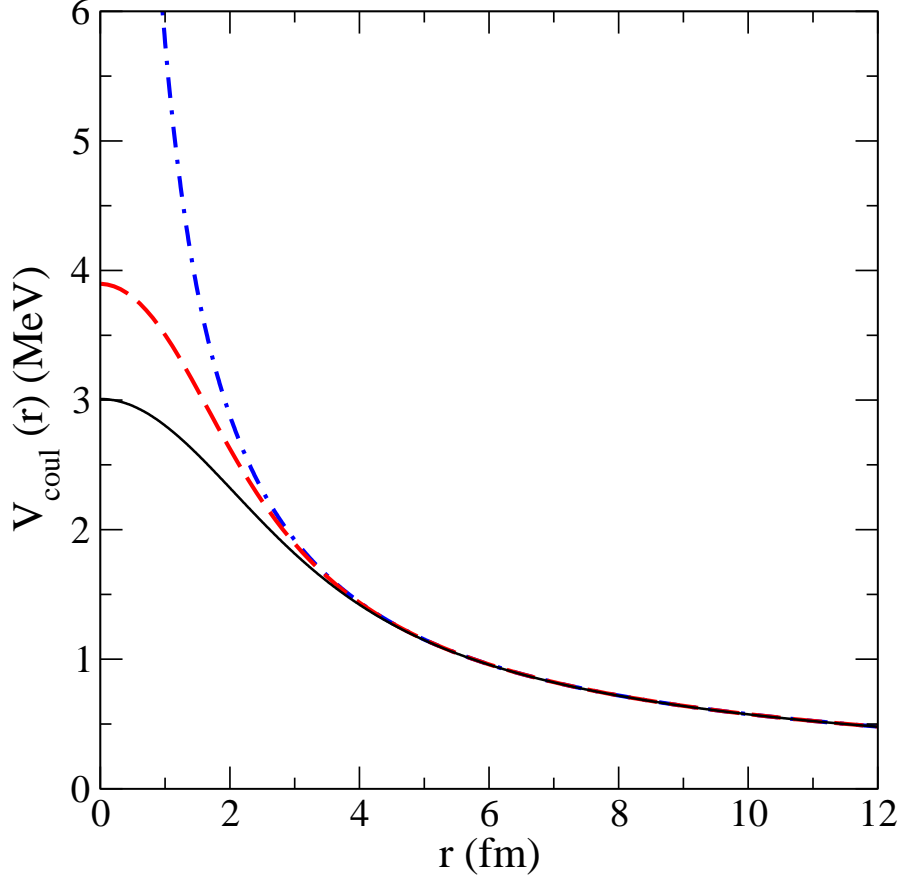


FIG. 6: (Color online) The Coulomb potentials for each of the three  $\alpha$ - ${}^6\text{He}$  interaction models.

The Coulomb potential for this point- $\alpha$  interacting with  ${}^6\text{He}$  with the selected 3pF charge distribution is depicted by the dashed curve in Fig. 6.

3. Both  $\alpha$  and  ${}^6\text{He}$  given by 3pF charge distributions.

For this case we fold the field given in Eq.(A7),  $(\mathcal{V}_\alpha(s))$ , with  $\delta e$  replacing the  $(2e)$ , with the 3pF charge distribution for the second  $\alpha$ . The geometry is as shown in Fig. 7 We seek a result for use in MCAS of  $V_{coul}(r)$  which, with  $s = \sqrt{r^2 + r'^2 - 2sr' \cos(\theta)}$ , is given by

$$V_{coul}(r) = 2\pi \int_0^\infty r'^2 f(r') \int_0^\pi \mathcal{V}_\alpha(s) \sin(\theta) d\theta. \quad (\text{A8})$$

The result is shown by the solid curve in Fig. 6.

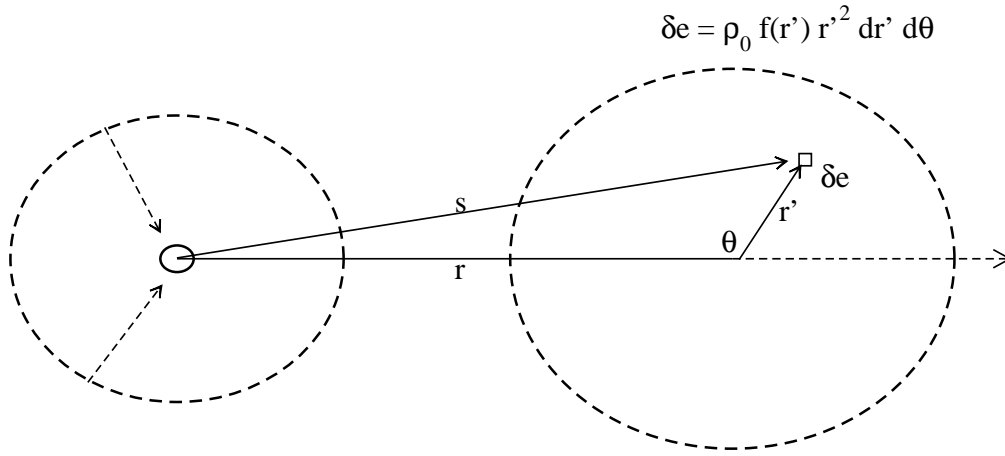


FIG. 7: (Color online) The geometry for both  $\alpha$  nuclei having a 3pF charge distribution.